

BARD1 reads H2A Lys-15 ubiquitination to direct homologous recombination (72 characters)

Authors: Jordan R. Becker^{1,3}, Gillian Clifford⁴, Clara Bonnet^{1,3}, Anja Groth^{5,6}, Marcus D. Wilson⁴, J. Ross Chapman^{1,2,3*}

Affiliations:

¹ Medical Research Council (MRC) Molecular Haematology Unit, Weatherall Institute of Molecular Medicine, University of Oxford, Oxford, OX3 9DS, UK.

² NIHR Biomedical Research Centre, University of Oxford, Oxford, OX3 9DU, UK.

³ Wellcome Centre for Human Genetics, University of Oxford, OX3 7BN, UK.

⁴ Wellcome Centre for Cell Biology, University of Edinburgh, Michael Swann Building, Kings Buildings, Mayfield Road, EH9 3BF, UK.

⁵ The Novo Nordisk Center for Protein Research (CPR), Faculty of Health Sciences, University of Copenhagen, 2200 Copenhagen, Denmark.

⁶ Biotech Research and Innovation Centre (BRIC), Faculty of Health Sciences, University of Copenhagen, 2200 Copenhagen, Denmark.

*Corresponding author: ross.chapman@imm.ox.ac.uk

Abstract:

Protein ubiquitination at sites of DNA double-strand breaks (DSBs) by RNF168 recruits BRCA1 and 53BP1^{1,2}, mediators of the homologous recombination (HR) and non-homologous end joining (NHEJ) DSB repair pathways, respectively³. While NHEJ relies on 53BP1 binding directly to ubiquitinated Lysine 15 on H2A-type histones (H2AK15ub)^{4,5} - an RNF168-dependent modification⁶ - how RNF168 promotes BRCA1 recruitment and function remains unclear. Here, we identify a tandem BRCT domain-associated ubiquitin-dependent recruitment motif (BUDR) in BARD1 – BRCA1's obligate partner protein – that by engaging H2AK15ub, recruits BRCA1 to DSBs. BARD1 BUDR disruption compromises HR and renders cells hypersensitive to PARP inhibition and cisplatin. We further show that BARD1 binds nucleosomes through multivalent interactions: coordinated binding of H2AK15ub and unmethylated H4 Lys20 (H4K20me0) by its adjacent BUDR and ankyrin repeat domains, respectively, provides high-affinity recognition of DNA lesions in replicated chromatin and promotes HR activities of the BRCA1-BARD1 complex. Finally, genetic epistasis experiments confirm that the need for BARD1-chromatin binding activities can be entirely relieved upon deletion of RNF168 or 53BP1. Thus, our results demonstrate that by sensing DNA damage-dependent and post-replication histone PTM states, BRCA1-BARD1 complexes coordinate 53BP1 pathway antagonization with HR promotion, establishing a simple paradigm for the governance of DSB repair pathway choice.

Main Text:

The equilibrium between accurate DNA double-strand break (DSB) repair by homologous recombination (HR), and error-prone DSB repair by non-homologous end joining (NHEJ) is controlled by the BRCA1 and 53BP1 proteins and their interplay with two histone post-translational modification (PTM) states. DNA damage recognition by both proteins involves ubiquitination of H2A-type histones at DSB sites by the DNA damage responsive E3 ubiquitin ligase RNF168^{1-3,6}. Chromatin engagement of 53BP1 and BRCA1 complexes also requires binding to histone H4 tails, through recognition of distinct lysine 20 methylation states that undergo DNA replication-dependent oscillations. Essential to its promotion of NHEJ, 53BP1 binds nucleosomes carrying histone H4 lysine 20 mono- and di- methylation (H4K20me1/2), histone PTMs highly abundant on old histones in pre- and post-replicative chromatin⁷⁻⁹. Conversely, BRCA1 complexes recognize H4 histones specifically when they are unmethylated at lysine 20 (H4K20me0), a state restricted to newly synthesized histones incorporated into chromatin during DNA replication¹⁰. H4K20me0 thereby recruits BRCA1 to post-replicative chromatin, where its promotion of HR is essential for genome stability and tumour suppression^{3,10}.

Specialized histone binding domains in BARD1 (BRCA1-Associated RING Domain Protein 1) - BRCA1's obligate interaction partner - and 53BP1, mediate histone H4 interactions. We recently showed the Ankyrin Repeat Domain (ARD) in BARD1 binds multiple residues in the H4 tail, and specifically Lysine-20 in its unmethylated state¹⁰, while the 53BP1 tandem-tudor domain (TTD) mediates the converse methylation-dependent interaction with H4K20me1/2⁷. To achieve specificity for chromatin proximal to DSBs, 53BP1 couples the binding of widespread H4K20me1/2 with recognition of the RNF168-dependent H2AK15ub PTM in DSB-proximal chromatin, using its ubiquitin-dependent recruitment motif (UDR), a TTD-proximal sequence that binds H2AK15ub and features of the nucleosome surface^{4,5}. The equivalent dependence of BRCA1 recruitment on RNF168 activity^{1,2} similarly implicates H2AK15ub recognition, however the mechanism linking BRCA1 complexes to this modification during HR have remained unknown.

Given that 53BP1-nucleosome interactions involve simultaneous binding to H4K20me1/2 and H2AK15ub, we considered whether the BRCA1-BARD1 complex might also possess sequences that bind H2AK15ub, and couple this to H4K20me0 recognition by the BARD1 ARD. BARD1 comprises an N-terminal RING, a central ARD, and a tandem BRCA1 C-terminal (BRCT) repeat domain at its C-terminus (Fig. 1a). Common to DNA damage responsive proteins, tandem BRCTs typically bind phosphoserine-containing peptide ligands in partner proteins¹¹⁻¹⁴. Putative phosphopeptide-binding residues are conserved in the BARD1 BRCTs, yet reportedly bind to Poly-ADP-ribose (PAR) chains induced at sites of DNA damage¹⁵. Despite this, we recently showed a PAR-binding defective point mutant of BARD1 (BARD1^{K619A}) was fully proficient in repairing olaparib-induced DNA lesions¹⁰. In agreement, mice homozygous for equivalent BARD1 BRCT mutations were not tumour prone and displayed a cellular proficiency for HR, dismissing a role for BRCT-dependent interactions with PAR or phospho-proteins in tumour suppression¹⁶. Nevertheless, when auxin-treated *BARD1^{AID/AID}* HCT-116 cells (herein referred to as *BARD1^{ΔΔ}* cells) – a cell-line engineered to encode biallelic auxin-dependent degron tags in the BARD1 C-terminus^{10,17} – were reconstituted with a BRCT repeat domain-deleted BARD1 transgene (BARD1^{ΔBRCT}), their hypersensitivity to olaparib (Fig. 1b) was consistent with their previously identified importance for HR¹⁸. Importantly, BARD1^{ΔBRCT} protein was expressed at endogenous levels and stabilized BRCA1 (Extended Data Fig. 1a), prompting us to consider a specific and undescribed function for the BARD1 BRCTs in HR.

To identify putative functional surfaces in the BARD1 BRCTs, we mapped sequence conservation onto a crystal structure of this domain¹⁹, and used this to prioritize highly-conserved solvent-exposed residues for mutagenesis (Fig. 1c). BARD1 transgenes bearing neutral or disruptive amino acid substitutions at 9 positions were then stably integrated into *BARD1^{AID/AID}* cells, and assayed for olaparib sensitivity following auxin-induced depletion of

endogenous BARD1 (Fig. 1d and Extended Data Fig. 1b). Interestingly, only mutations within a focused cluster of 3 conserved residues - Arg-705, Asp-712 and Gln-715 - conferred olaparib sensitivity (Fig. 1d). These all mapped to the loop formed between beta-sheets 2 and 3 of BARD1's second BRCT (inter- β 2'- β 3' loop, Fig. 1e), a protruding feature comprising three 3_{10} helices previously noted to be unique among BRCTs¹⁹. The observation that all three mutant BARD1 proteins were stable (Extended Data Fig. 1b-c), yet potentiated olaparib hypersensitivity, indicated a direct role for the inter- β 2'- β 3' loop in HR.

We noted that BRCT₂ inter- β 2'- β 3' loop mutants exhibited olaparib sensitivity profiles equivalent to ARD mutated BARD1^{ARD 3A} expressing cell lines (Fig. 2a and Extended Data Fig. 2a), and considered that the BARD1 ARD and BRCTs might be functionally interconnected. Consistent with this notion, ARD 3A mutations did not synergize with the D712A inter- β 2'- β 3' loop mutation in increasing cellular hyper-sensitivity to olaparib (Fig. 2b and Extended Data Fig. 2b) or cisplatin (Fig. 2c and Extended Data Fig. 2c). We thus used *BARD1*^{ΔΔ} cells complemented with either wild type, *BARD1*^{ARD 3A}, *BARD1*^{D712A}, or *BARD1*^{ARD 3A/D712A} double mutant BARD1 transgenes to assess whether cooperation between the ARD and tandem BRCT domains in BARD1 was necessary for BRCA1-BARD1 recruitment to DSB sites. High content imaging of BRCA1 ionizing radiation induced foci (IRIF) was combined with immunofluorescence intensity-labelling of H4K20me0, to quantify BRCA1 recruitment in H4K20me0-high cell populations where IR-induced BRCA1 recruitment is highest¹⁰. Control (GST) complemented BARD1 deficient cells exhibited profound BRCA1 recruitment defects that were suppressed upon wild type BARD1 complementation (Fig. 2d-e and Extended Data Fig. 2d-e). However, only very low frequencies of BRCA1 IRIF were observed in cells complemented with the *BARD1*^{ARD 3A}, *BARD1*^{D712A}, or *BARD1*^{ARD 3A/D712A} transgenes (Fig. 2d-e and Extended Data Fig. 2d-e). This confirmed a requirement for ARD-BRCT cooperation in the recruitment of BRCA1. We suspected that residual BRCA1 IRIF detected in ARD and BRCT mutant-complemented cells were dependent on the BRCA1-A complex: a protein complex composed of BRCC36, ABRAXAS, BRE, MERIT40, and RAP80, which recruits BRCA1-BARD1 to DNA damage sites via RAP80-mediated interactions with Lysine-63-linked polyubiquitin chains²⁰⁻²⁴, yet is dispensable for BRCA1-dependent HR²⁵. Consistent with previous reports^{25,26}, BRCA1 IRIF frequencies in wild type BARD1 complemented *BARD1*^{ΔΔ} cells were only modestly reduced by deletion of RAP80 (Fig. 2f-g). By contrast, BRCA1 IRIF were ablated in *RAP80*^{-/-} *BARD1*^{ΔΔ} cells complemented with the *BARD1*^{D712A}, *BARD1*^{ARD 3A}, and *BARD1*^{ARD 3A, D712A} double mutants (Fig. 2f-g and Extended Data Fig. 2f-g). Thus, BARD1's ARD-BRCT domains recruit BRCA1 to DSBs independently of RAP80 and BRCA1-A. Notably however, *BARD1*^{D712A} expression significantly improved the survival of olaparib-treated *RAP80*^{+/+} *BARD1*^{ΔΔ} cells, yet offered no survival benefit when expressed in *RAP80*^{-/-} *BARD1*^{ΔΔ}

cells (Fig. 2h). Thus, our results suggest that in the absence of BARD1-dependent recruitment of BRCA1-BARD1, residual RAP80-dependent recruitment of BRCA1 makes a significant, albeit partial, positive contribution to DNA repair.

Next, to examine the contribution of the BARD1 ARD-BRCT domains to HR, we quantified the effect of the BARD1^{D712A}, BARD1^{ARD 3A} mutation on RAD51 recruitment into IRIF. In contrast to wild type BARD1-complemented *BARD1*^{Δ/Δ} cells, in which RAD51 frequencies were fully restored, neither complementation with BARD1^{D712A}, BARD1^{ARD 3A} nor BARD1^{ARD 3A, D712A} improved RAD51 recruitment into IRIF when compared to GST-complemented control cells (Fig. 2i-j). These results collectively confirm that the ARD-BRCT domain architecture in BARD1 functions as BRCA1's primary recruitment module during HR.

Interdependence between the BARD1 ARD and BRCTs suggested their cooperation in chromatin binding at DSB sites. We therefore speculated the BARD1 C-terminal domain architecture might couple H4K20me0 and H2AK15ub binding in a manner analogous to the TTD-UDR domains of 53BP1. If the BARD1 BRCT repeats interacted with H2AK15ub, we reasoned that they might rescue the recruitment of a UDR mutated IRIF-forming fragment of 53BP1²⁷ (amino acids 1220-1711) that cannot bind H2AK15ub^{4,5}. We tested this hypothesis by expressing chimeric proteins in which wild-type or D712A mutant versions of the BARD1 BRCT repeats were fused C-terminal to wild-type or UDR-mutated fragments of 53BP1^{aa1220-1711}, and examined their ability to form IRIF in *53BP1*^{-/-} *BARD1*^{Δ/Δ} cells. The 53BP1^{aa1220-1711::BARD^{BRCT1-2}} fusion proteins readily formed IRIF that were completely ablated when recruitment-neutralizing UDR (L1619A^{4,27}) and BARD1 BRCT (D712A) mutations were both present (Extended Data Fig. 3a-b). However, the ability of equivalent proteins bearing either the wild type UDR or a BARD1 BRCT domain to form IRIF (Extended Data Fig. 3a; +D712A and +L1616A panels, respectively), strongly suggested that the BARD1 BRCT repeats, akin to the 53BP1 UDR⁴, might recognize H2AK15ub at DSB sites.

To directly test whether the BARD1 BRCT repeats bind H2AK15ub labelled nucleosomes, a glutathione S-transferase (GST) fusion protein fragment encoding the BARD1^{ARD-BRCT} was recombinantly expressed and purified (Extended Data Fig. 3c). GST pull-downs were then performed following incubation with recombinant nucleosomes that were either unmodified, chemically methylated at H4K20 (H4Kc20me2), chemically ubiquitinated at H2AK15 (H2AKc15ub), or modified at both positions (Extended Data Fig. 3d-e). In these experiments, interactions between the BARD1^{ARD-BRCT} fragment and nucleosomes were strongly stimulated by the presence of H2AKc15ub, yet inhibited when H4Kc20me2 was also present (Fig. 3a). In contrast, the presence of both histone PTMs was required when nucleosome binding experiments were performed with a control recombinant GST fusion polypeptide encoding the 53BP1 TTD-UDR (Fig. 3a), consistent with previous observations^{4,5,28}. The inhibitory effect of H4K20-methylation on the binding of BARD1 to

H2AK15ub-labelled nucleosomes was furthermore confirmed by electrophoretic mobility shift assay (EMSA), in which a recombinant monomeric 6xHis-MBP-BARD1^{ARD-BRCT} fragment exhibited over 4-fold higher affinity for H2AK15ub-labelled nucleosomes when they were not methylated on H4K20 (Fig. 3b and Extended Data Fig. 3f). The inverse was seen for a GST-53BP1^{TTD-UDR} fragment, where H4K20 dimethylation stimulated binding to H2AK15ub-labelled nucleosomes by EMSA (Extended Data Fig. 3f), as expected^{4,5,7}. Lastly, interactions between H2AK15ub-modified nucleosomes and GST-BARD1^{ARD-BRCT} fragments, were sensitive to the ARD 3A and D712A mutations alone, and in combination (Fig. 3c and Extended Data Fig. 3g). These results collectively confirm that the ARD and BRCT domains cooperate in nucleosome binding, and implied a specificity for RNF168-dependent H2AK15ub. H2AK15ub-directed specificity was furthermore confirmed in nucleosome pulldown experiments where ubiquitin was instead conjugated to H2A Lysine 119 (H2AK119ub), a Polycomb Repressive Complex 1 (PRC1)-dependent modification present on 5-15% of all H2A in vertebrate cells²⁹. In contrast to its high affinity for H2AK15ub, we did not detect an interaction between recombinant GST-BARD1^{ARD-BRCT} polypeptides and H2AK119ub-containing nucleosomes, indicating a selectivity for H2AK15ub (Fig. 3d). Thus, the BARD1 BRCT repeats are a reader of DNA-damage dependent H2AK15ub. Given the analogous functioning ubiquitin-dependent recruitment motif (UDR) in 53BP1, which also binds H2AK15ub^{4,5,28}, we named the inter-β2'-β3' loop of BARD1 the BRCT-associated ubiquitin-dependent recruitment motif (BUDR).

The RNF168 E3 ubiquitin ligase catalyzes ubiquitination of H2AK15 at sites of DSBs⁶, promoting BRCA1 and 53BP1 recruitment into IRIF^{1,2,6}. Consistently, RNF168-deletion in *BARD1^{AID/AID}* cells near-completely blocked BRCA1 and 53BP1 recruitment (Extended Data Fig. 4a-d). This effect was specific, as cells deleted of the PRC1 E3 ubiquitin ligases (RING1A and RING1B), were fully proficient in supporting 53BP1 and BRCA1 IRIF, despite ablating H2AK119ub (Extended Data Fig. 4e-f). Likewise, *BARD1^{ΔΔ}* cells complemented with the BARD1^{R99E} mutant defective for H2A Lys-127 ubiquitination^{30,31} supported normal frequencies of BRCA1 and 53BP1 IRIF (Extended Data Fig. 4g). Thus, BRCA1-BARD1 recruitment to DNA damage sites does not involve polycomb- and BRCA1-BARD1- directed H2A ubiquitination events.

In cell viability assays performed in the presence of increasing doses of olaparib, RNF168-deletion dramatically increased the survival of *BARD1^{ΔΔ}* cells (Fig 4a-b). However, olaparib resistance in *RNF168^{-/-} BARD1^{ΔΔ}* cells was only fully rescued to levels comparable to non-auxin treated *RNF168^{-/-} BARD1^{AID/AID}* control cells when they were additionally complemented with wild-type BARD1 (Fig. 4a-b). Remarkably, an equivalent rescue also occurred when *RNF168^{-/-} BARD1^{ΔΔ}* cells were complemented with BARD1^{ARD 3A} or BARD^{D712A} expression (Fig. 4a-b). This indicated a genetic epistasis between loss of RNF168-dependent

H2AK15ub and mutations affecting BARD1's ability to recognize this mark. In complete agreement, IRIF formed by a fragment of BARD encompassing its minimal chromatin-binding domains fused to the monomeric GFP variant mClover2 (mC2-ARD-BRCT) were equally disrupted by RNF168-deletion and ARD-3A/BUDR mutations in live cell imaging experiments (Fig. 4c). It is noteworthy, however, that mC2-ARD-BRCT IRIF did not withstand fixation procedures, suggesting other nucleosome binding features of the BRCA1-BARD1 complex³² may stabilise ARD-BRCT-dependent chromatin interactions.

Given the vital function H2AK15ub also plays in recruiting 53BP1 to chromatin at DSB sites, and BRCA1's importance for antagonizing 53BP1-interactions with post-replicative chromatin^{10,33,34}, we hypothesized that BARD1's chromatin-reader activities may have evolved to counteract 53BP1 pathway activity. In agreement with this notion, RAD51 IRIF were diminished in *BARD1*^{ΔΔ} cells, restored in *53BP1*^{-/-} *BARD1*^{ΔΔ} cells, and no further increases accompanied reconstitution of wild-type or mutant BARD1 protein expression (Extended Data Fig. 5a-d). However, despite this rescue of RAD51 recruitment, *53BP1*^{-/-} *BARD1*^{ΔΔ} cells retained significant sensitivity to both olaparib and cisplatin treatments (IC₅₀ (olaparib) ~63 nM, Fig. 4d-g), a result that suggested incomplete restoration of HR. In stark contrast, resistance to both cisplatin and olaparib treatments was fully restored in *53BP1*^{-/-} *BARD1*^{ΔΔ} cells upon reconstitution with BARD1^{D712A} and BARD1^{ARD 3A} mutant proteins (IC₅₀ (olaparib) >1 μM), which was comparable to cells reconstituted with wild type BARD1 (Fig. 4d-g and Extended Data Fig. 5e-h). In summary, the equal effect of 53BP1- and RNF168- loss in restoring HR functionality to cells proficient or deficient in BARD1-chromatin interactions is consistent with 53BP1 pathway inhibition representing the primary role for BARD1's interactions with H4K20me0/H2AK15ub marked nucleosomes. Our results also suggest that BRCA1-BARD1 complexes exert important functions that do not require BARD1-mediated chromatin-binding, perhaps partly explaining the incomplete phenotypic suppression by 53BP1-deletion in mice bearing severe *Brca1* loss-of-function alleles^{35,36}.

Altogether, our results answer the long-standing question of how the DNA damage-associated H2AK15ub histone modification promotes BRCA1-BARD1 complex recruitment, where it coordinates HR promotion with inhibition of 53BP1-dependent NHEJ. In identifying the BARD1 BRCT repeats as a specific receptor for H2AK15ub, we also reveal a conserved and simple principle governing the equilibrium between competing DSB repair pathways, in which two histone PTM states – one cell-cycle regulated (H4K20±me1/2), and one DNA-damage dependent (H2AK15±ub) – specify bivalent interactions with the reader domains of distinct repair pathway mediator proteins (Fig 4h-i). The shared affinity of BARD1 ARD-BUDR and 53BP1 TTD-UDR architectures for H2AK15ub-modified nucleosomes, yet inverse affinities for H4K20 methylation, explains the respective preferences of these proteins for

239 DSB-associated chromatin in post- and pre-replicated regions of the genome, and the
240 establishment of DSB repair pathway choice.
241

References:

- 1 Doil, C. *et al.* RNF168 Binds and Amplifies Ubiquitin Conjugates on Damaged Chromosomes to Allow Accumulation of Repair Proteins. *Cell* **136**, 435-446, doi:10.1016/j.cell.2008.12.041 (2009).
- 2 Stewart, G. S. *et al.* The RIDDLE Syndrome Protein Mediates a Ubiquitin-Dependent Signaling Cascade at Sites of DNA Damage. *Cell* **136**, 420-434, doi:10.1016/j.cell.2008.12.042 (2009).
- 3 Hustedt, N. & Durocher, D. The control of DNA repair by the cell cycle. *Nature Cell Biology* **19**, 1-9, doi:10.1038/ncb3452 (2017).
- 4 Fradet-Turcotte, A. *et al.* 53BP1 is a reader of the DNA-damage-induced H2A Lys 15 ubiquitin mark. *Nature* **499**, 50-54 (2013).
- 5 Wilson, M. D. *et al.* The structural basis of modified nucleosome recognition by 53BP1. *Nature* **536**, 100-103 (2016).
- 6 Mattioli, F. *et al.* RNF168 Ubiquitinates K13-15 on H2A/H2AX to Drive DNA Damage Signaling. *Cell* **150**, 1182-1195, doi:<https://doi.org/10.1016/j.cell.2012.08.005> (2012).
- 7 Botuyan, M. V. *et al.* Structural basis for the methylation state-specific recognition of histone H4-K20 by 53BP1 and Crb2 in DNA repair. *Cell* **127**, 1361-1373 (2006).
- 8 Bothmer, A. *et al.* Regulation of DNA end joining, resection, and immunoglobulin class switch recombination by 53BP1. *Mol. Cell* **42**, 319-329 (2011).
- 9 Dimitrova, N., Chen, Y.-C. M., Spector, D. L. & de Lange, T. 53BP1 promotes non-homologous end joining of telomeres by increasing chromatin mobility. *Nature* **456**, 524 (2008).
- 10 Nakamura, K. *et al.* H4K20me0 recognition by BRCA1–BARD1 directs homologous recombination to sister chromatids. *Nature Cell Biology* **21**, 311-318, doi:10.1038/s41556-019-0282-9 (2019).
- 11 Manke, I. A., Lowery, D. M., Nguyen, A. & Yaffe, M. B. BRCT Repeats As Phosphopeptide-Binding Modules Involved in Protein Targeting. *Science* **302**, 636, doi:10.1126/science.1088877 (2003).
- 12 Yu, X., Chini, C. C. S., He, M., Mer, G. & Chen, J. The BRCT Domain Is a Phospho-Protein Binding Domain. *Science* **302**, 639, doi:10.1126/science.1088753 (2003).
- 13 Glover, J. N. M., Williams, R. S. & Lee, M. S. Interactions between BRCT repeats and phosphoproteins: tangled up in two. *Trends in Biochemical Sciences* **29**, 579-585, doi:<https://doi.org/10.1016/j.tibs.2004.09.010> (2004).
- 14 Wu, Q., Jubb, H. & Blundell, T. L. Phosphopeptide interactions with BRCA1 BRCT domains: More than just a motif. *Prog Biophys Mol Biol* **117**, 143-148, doi:10.1016/j.pbiomolbio.2015.02.003 (2015).
- 15 Li, M. & Yu, X. Function of BRCA1 in the DNA Damage Response Is Mediated by ADP-Ribosylation. *Cancer Cell* **23**, 693-704, doi:<https://doi.org/10.1016/j.ccr.2013.03.025> (2013).
- 16 Billing, D. *et al.* The BRCT Domains of the BRCA1 and BARD1 Tumor Suppressors Differentially Regulate Homology-Directed Repair and Stalled Fork Protection. *Molecular Cell* **72**, 127-139.e128, doi:<https://doi.org/10.1016/j.molcel.2018.08.016> (2018).
- 17 Natsume, T., Kiyomitsu, T., Saga, Y. & Kanemaki, M. T. Rapid Protein Depletion in Human Cells by Auxin-Inducible Degron Tagging with Short Homology Donors. *Cell Reports* **15**, 210-218, doi:<https://doi.org/10.1016/j.celrep.2016.03.001> (2016).
- 18 Laufer, M. *et al.* Structural requirements for the BARD1 tumor suppressor in chromosomal stability and homology-directed DNA repair. *Journal of Biological Chemistry* **282**, 34325-34333, doi:10.1074/jbc.M705198200 (2007).
- 19 Birrane, G., Varma, A. K., Soni, A. & Ladias, J. A. A. Crystal Structure of the BARD1 BRCT Domains. *Biochemistry* **46**, 7706-7712, doi:10.1021/bi700323t (2007).
- 20 Sobhian, B. *et al.* RAP80 Targets BRCA1 to Specific Ubiquitin Structures at DNA Damage Sites. *Science* **316**, 1198, doi:10.1126/science.1139516 (2007).

- 21 Wang, B. *et al.* Abraxas and RAP80 Form a BRCA1 Protein Complex Required for the DNA Damage Response. *Science* **316**, 1194, doi:10.1126/science.1139476 (2007).
- 22 Kim, H., Chen, J. & Yu, X. Ubiquitin-Binding Protein RAP80 Mediates BRCA1-Dependent DNA Damage Response. *Science* **316**, 1202, doi:10.1126/science.1139621 (2007).
- 23 Sims, J. J. & Cohen, R. E. Linkage-specific avidity defines the lysine 63-linked polyubiquitin-binding preference of rap80. *Mol Cell* **33**, 775-783, doi:10.1016/j.molcel.2009.02.011 (2009).
- 24 Sato, Y. *et al.* Structural basis for specific recognition of Lys 63-linked polyubiquitin chains by tandem UIMs of RAP80. *The EMBO Journal* **28**, 2461-2468, doi:10.1038/emboj.2009.160 (2009).
- 25 Hu, Y. *et al.* RAP80-directed tuning of BRCA1 homologous recombination function at ionizing radiation-induced nuclear foci. *Genes & Development* **25**, 685-700 (2011).
- 26 Shao, G. *et al.* MERIT40 controls BRCA1-Rap80 complex integrity and recruitment to DNA double-strand breaks. *Genes & development* **23**, 740-754, doi:10.1101/gad.1739609 (2009).
- 27 Zgheib, O., Pataky, K., Brugger, J. & Halazonetis, T. D. An oligomerized 53BP1 tudor domain suffices for recognition of DNA double-strand breaks. *Mol. Cell. Biol.* **29**, 1050-1058 (2009).
- 28 Hu, Q., Botuyan, M. V., Cui, G., Zhao, D. & Mer, G. Mechanisms of Ubiquitin-Nucleosome Recognition and Regulation of 53BP1 Chromatin Recruitment by RNF168/169 and RAD18. *Molecular Cell* **66**, 473-487.e479, doi:10.1016/j.molcel.2017.04.009 (2017).
- 29 Cao, J. & Yan, Q. Histone Ubiquitination and Deubiquitination in Transcription, DNA Damage Response, and Cancer. *Frontiers in Oncology* **2**, 26 (2012).
- 30 Densham, R. M. *et al.* Human BRCA1-BARD1 ubiquitin ligase activity counteracts chromatin barriers to DNA resection. *Nature Structural & Molecular Biology* **23**, 647, doi:10.1038/nsmb.3236 (2016).
- 31 Kalb, R., Mallery, Donna L., Larkin, C., Huang, Jeffrey T. J. & Hiom, K. BRCA1 Is a Histone-H2A-Specific Ubiquitin Ligase. *Cell Reports* **8**, 999-1005, doi:<https://doi.org/10.1016/j.celrep.2014.07.025> (2014).
- 32 Witus, S. R. *et al.* BRCA1/BARD1 site-specific ubiquitylation of nucleosomal H2A is directed by BARD1. *Nature Structural & Molecular Biology* **28**, 268-277, doi:10.1038/s41594-020-00556-4 (2021).
- 33 Chapman, J. R., Sossick, A. J., Boulton, S. J. & Jackson, S. P. BRCA1-associated exclusion of 53BP1 from DNA damage sites underlies temporal control of DNA repair. *Journal of Cell Science* **125**, 3529 (2012).
- 34 Pellegrino, S., Michelena, J., Teloni, F., Imhof, R. & Altmeyer, M. Replication-Coupled Dilution of H4K20me2 Guides 53BP1 to Pre-replicative Chromatin. *Cell Reports* **19**, 1819-1831, doi:<https://doi.org/10.1016/j.celrep.2017.05.016> (2017).
- 35 Nacson, J. *et al.* BRCA1 Mutation-Specific Responses to 53BP1 Loss-Induced Homologous Recombination and PARP Inhibitor Resistance. *Cell reports* **24**, 3513-3527.e3517, doi:10.1016/j.celrep.2018.08.086 (2018).
- 36 Chen, J. *et al.* 53BP1 loss rescues embryonic lethality but not genomic instability of BRCA1 total knockout mice. *Cell Death & Differentiation*, doi:10.1038/s41418-020-0521-4 (2020).

Acknowledgments: We thank all members of the Chapman lab for discussions, Daniel Durocher for plasmid reagents, Neil Johnson for discussions regarding unpublished data and Tim Humphrey for comments on the manuscript. This work was funded by Cancer Research UK (CRUK) Career Development Fellowship (C52690/A19270 to JRC) which also provided

salary support to JRB, and CRUK Oxford Centre funding (C5255/A18085 to JRB and JRC). JRB's salary is currently provided by a Ruth L. Kirschstein NRSA Individual Postdoctoral Fellowship (F32) (NIH/NCI - F32CA239339). The Chapman lab is also supported by the Medical Research Council (MRC - MR/R017549/1), the MRC Molecular Haematology Unit (MRC MHU, UK) and the National Institute for Health Research (NIHR) Oxford Biomedical Research Centre (BRC). JRC holds a Lister Institute Research Prize Fellowship. The Wellcome Centre for Human Genetics is supported by Wellcome core award 090532/Z/09/Z. CB was sponsored by an ERASMUS+ internship. MDW's work is supported by the Wellcome Trust (210493), Medical Research Council (T029471/1), and the University of Edinburgh. The Wellcome Centre for Cell Biology is supported by core funding from the Wellcome Trust (203149). AG's research is supported by the Lundbeck Foundation [R198-2015-269; R313-2019-448], the European Research Council [ERC CoG no. 724436] and Independent Research Fund Denmark [7016-00042B; 4092-00404B]. Research at CPR is supported by the Novo Nordisk Foundation [NNF14CC0001]. We also acknowledge the BHF Centre of Research Excellence, Oxford (RE/13/1/30181), and the WHG Cellular Imaging core for equipment access and support.

Author Contributions: JRB designed and analysed the majority of experiments, and supervised experiments performed by CB. MDW and GC undertook and analysed all *in vitro* nucleosome binding experiments. The project was initiated in collaboration with AG. JRC conceived and supervised the project, designed and analysed experiments. JRB and JRC co-wrote the manuscript, with author input.

Competing interests: AG is co-founder and CSO in Ankrin Therapeutics. No other authors have competing interests.

Data Availability: All data is available in the main text or extended data. Raw data for Figures 2a-c, 2e, 2g, 2h, 2j, 3a, 3c, 3d, 4a, 4b, 4d-g, Extended Data Figures 1a-c, 2a-c, 2e, 2g-i, 3a, 3c-g, 4b, 4d-g, and 5b-h are available in the source data file.

Materials availability: Material requests should be addressed to JRC.

Figures Legends

Fig. 1. Residues in the inter- β 2'- β 3' loop of BARD1 BRCT2 are essential for HR. (A) *BARD1* domain map with ARD 3A (N470A E467A D500A) and K619A mutations indicated. **(B)** Survival of indicated *BARD1*^{AID/AID} cells grown in the presence of olaparib. Cultures were supplemented with doxycycline (2 μ g/ml) for 24 h before auxin addition (1 mM IAA). Olaparib (500 nM) was added 1 h after IAA. Cells were stained following a 10 day olaparib treatment. Representative data, $n=3$ biological experiments. **(C)** Space-filling (*top*) and ribbon (*bottom*) models of the BARD1 tandem BRCT crystal structure (PDB ID: 2NTE) pseudo-coloured to indicate amino acid conservation. Red dashed ovals indicate the inter- β 2'- β 3' loop. **(D)** As in (B). Representative data, $n=3$ biological experiments. **(E)** The inter- β 2'- β 3' loop with amino acid side-chains represented.

Fig. 2. Ankyrin and BRCT repeat domains in BARD1 co-recruit BRCA1 during HR. (A-C) Survival of indicated *BARD1*^{AID/AID} cell lines grown for 7 days in the presence of IAA (1 mM), doxycycline (2 μ g/ml), and the indicated doses of olaparib or cisplatin. Resazurin cell viability assay, $n=3$ biological experiments, mean \pm SD. **(D)** Immunofluorescent microscopy of BRCA1 IRIF in H4K20me0-positive *BARD1*^{AID/AID} cell lines. Cultures supplemented with doxycycline (2 μ g/ml for 24 h) before IAA (1 mM) addition, were irradiated after 2 h (5 Gy), and fixed 2 h later. Scale bar, 5 μ m. Representative of $n=2$ biological experiments. **(E)** *Top*: quantification of BRCA1 IRIF from (D). Boxes, median \pm 25th-75th percentiles; whiskers indicate 10th-90th percentiles. BRCA1 foci measurements are made for nuclei in the top quartile of H4K20me0 integrated staining intensity (≥ 171 nuclei per condition). Integrated intensity and foci quantifications were made using CellProfiler. Significance was determined by two-sided Kruskal-Wallis H test with Dunn's correction for multiple comparisons (**** $p \leq 0.0001$). *Bottom*: Mean number of BRCA1 foci per cell from two independent experiments. **(F and G)** Same as in (D-E) in *RAP80*^{-/-} cells. ≥ 178 nuclei per condition. **(H)** Survival of indicated *BARD1*^{AID/AID} cell lines grown for 7 days in the presence of olaparib. Cultures were supplemented with doxycycline (2 μ g/ml) for 24 h before IAA (1 mM) and olaparib addition. Resazurin cell viability assay, $n=3$ biological experiments, mean \pm SD. **(I)** Immunofluorescent microscopy of RAD51 IRIF in *BARD1*^{AID/AID} cells expressing the indicated transgenes. Cultures supplemented with doxycycline (2 μ g/ml, 24 h) before IAA addition (1 mM, 2 h), were irradiated (5 Gy) and fixed 2 h later. Scale bar, 5 μ m. Representative of $n=3$ biological experiments. **(J)** *Top*: Quantification of Rad51 foci per cell from (I). ≥ 255 nuclei per condition. Boxes, median \pm 25th-75th percentiles; whiskers indicate 10th-90th percentiles. Significance was determined by two-sided Kruskal-Wallis H test with Dunn's correction for multiple comparisons (**** $p \leq 0.0001$).

Representative of $n=3$ biological experiments. *Bottom*: Mean number of RAD51 IRIF from three independent biological experiments \pm SD.

Fig. 3. Specific recognition of ubiquitinated Lysine 15 on histone H2A by the BARD1 BRCT repeats. (A) Immunoblots from pull-down assay using GST tagged BARD1^{ARD-BRCT} and 53BP1^{TTD-UDR} fragments immobilised on glutathione affinity beads and incubated with recombinant nucleosome variants. Nucleosomes were either modified with dimethyl-lysine analogs at H4 position 20 and/or chemically ubiquitinated at H2A position 15. Representative of $n=3$ independent experiments. (B) Quantification of EMSA experiments in which H2AKc15ub or H2AKc15ubH4Kc20me2 modified nucleosomes (or control DNA) were incubated with increasing concentrations of 6xHis-MBP tagged BARD1^{ARD-BRCT}. Complexes were resolved by native PAGE and visualized using Diamond DNA stain. Includes data from $n=3$ independent experiments \pm SEM. (C) Immunoblots from pull-down assay using tandem GST, GST tagged BARD1^{ARD-BRCT} wild type (WT) and indicated point mutants. Pull-down was performed on immobilized GST tagged proteins incubated with recombinant nucleosomes chemically ubiquitinated at position 15 on H2A. ARD 3A, comprises mutations (N470A E467A D500A) in the Ankyrin repeat domain while D712A is in tandem BRCT domain. Representative of $n=3$ independent experiments. (D) Immunoblots from pull-down assay using GST tagged BARD1^{ARD-BRCT} fragments immobilised on glutathione affinity beads, and incubated with recombinant nucleosome variants. Nucleosomes were chemically ubiquitinated at H2A position 15 or 119. Representative of $n=3$ independent experiments.

Fig. 4. Control of DSB repair pathway selection by two histone modification states and their readers. (A-B) Survival of indicated *BARD1*^{AID/AID} cell lines grown for 7 days in the presence of indicated olaparib doses. Cultures were grown in doxycycline (2 μ g/ml) for 24h before IAA (1 mM) or DMSO (carrier control) addition, and subsequent olaparib addition (at 25 h). 7 days later, cell viability was measured by resazurin assay. $n=3$ biological experiments, mean \pm SD. (C) *BARD1*^{AID/AID} cells expressing an mC2-ARD-BRCT transgene or derivatives with ARD 3A or D712A mutations were grown in doxycycline (2 μ g/ml, 24 h) before IAA (1 mM) addition. 2 h later, cultures were irradiated (10 Gy) and live imaging began 60 min after irradiation. Scale bar, 10 μ m. Representative of $n=2$ independent experiments. (D-G) Survival of indicated *BARD1*^{AID/AID} cell lines grown for 7 days in the presence of indicated doses of olaparib or cisplatin. Cultures were grown in doxycycline (2 μ g/ml) for 24h before IAA (1 mM) or DMSO (carrier control) addition, and subsequent olaparib or cisplatin addition (at 25 h). 7 days later, cell viability was measured by resazurin assay. $n=3$ biological experiments, mean \pm SD. Data in Fig. 4D and Fig. 2A was collected from common experiments, with indicated cell-

452 lines displayed separately for clarity. **(E)** Propose model for bivalent nucleosome recognition
453 by BARD1. **(F)** Logic gate depicting how combinatorial H2AK15 and H4K20 PTM states
454 govern DSB repair pathway choice.
455
456

Materials and Methods

Cell lines and culture conditions

BARD1^{AID/AID} cells lines were generated by biallelic knock-in of auxin-inducible degron tags at the C-terminus of the endogenous *BARD1* loci in the adult male HCT116 colorectal carcinoma cells (parental cell line was a gift from I. Tomlinson, RRID: CVCL_0291) carrying doxycycline-inducible copies of OsTIR1 integrated at the AAVS1 loci as previously described⁸. All *BARD1^{AID/AID}* and derivative cell lines were maintained in Dulbecco's modified Eagle medium (DMEM)-high glucose (Sigma-Aldrich, D6546) supplemented with 10% FBS, Pen-Strep, and 2 mM L-glutamine. Cultures were maintained at 37°C with 5% CO₂.

To generate lentivirus for stable transgene complementation, HEK 293T female embryonic kidney cells (Obtained from Francis Crick Institute Cell Services, RRID: CVCL_0063) were co-transfected with a lentiviral vector encoding the transgene of interest, pHDM-tat1b, pHDM-G, pRC/CMV-rev1b, and pHDM-Hgpm2 using 1.29 µg polyethylenimine per µg of DNA in Opti-MEM (Thermo Fisher, 31985062). Viral supernatants were harvested at 48 h and 72 h after transfection, syringe filtered (0.45- µm), and immediately used to transduce target cells populations in the presence of 4 µg/ml polybrene. Transduced populations were selected with antibiotic beginning 24 h after the last round of transduction until a non-transduced control population was completely dead. Stably transduced cell lines were maintained in the presence of selective antibiotic.

All knock-out cell lines were generated by CRISPR-Cas9. Gene-specific gRNAs were integrated into pSpCas9(BB)-2A-GFP (PX458) (Addgene #48138) and 2 µg of plasmid was electroporated into 10⁶ cells using a Lonza 4D-Nucleofector™ according to the manufacturer's protocol for HCT116 cells. GFP positive cells were sorted 24 h after electroporation using a Sony SH800 cell sorter with the brightest 5% being pooled for recovery in medium containing 50% FBS for 4 days. Sorted populations were then seeded at low density and individual clones were isolated after 10 days outgrowth. Individual clones were validated by western blot and sequencing. All cell lines were validated as described in the reporting checklist, and tested for mycoplasma contamination upon entering the laboratory.

Survival experiments

To generate survival curves for *BARD1^{AID/AID}* and derivative cell lines, 300 cells per well were seeded in the presence of doxycycline (2 µg/ml) in triplicate for each drug concentration in a 96-well plate. Each cell line was plated in duplicate for plus and minus IAA conditions. After 24 h, IAA (1 mM) or carrier (DMSO) was added. One hour following IAA addition, olaparib or cisplatin was added to the indicated final concentrations. Seven days after drug addition, the medium was replaced with phenol red-free DMEM (Thermo Fisher,

21063-029) supplemented with 10% FBS, Pen-Strep, 2 mM L-glutamine, and 10 µg/ml resazurin (Sigma-Aldrich, R7017). Plates were then returned to the incubator for 2-4 h or until the growth medium in untreated control wells began to develop a pink color. Relative fluorescence was measured with a BMG LABTECH CLARIOstar plate reader. The mean of three technical repeats after background subtraction was taken as the value for a biological repeat and three biological repeats were performed for each experiment. All survival curves presented in this study represent the mean of three biological repeats ±SD.

For survival experiments analyzed by crystal violet staining, 10⁴ cells were seeded per well of a 6-well plate in triplicate for each cell line in the presence of doxycycline (2 µg/ml). After 24 h, IAA (1 mM) or carrier (DMSO) was added. One hour following IAA addition, olaparib was added to the indicated final concentrations. Ten days after plating, the growth medium was removed and the cells were washed briefly with PBS before the addition of crystal violet stain (0.5% crystal violet in 25% methanol). Cells were stained for 5 minutes, washed with ddH₂O and dried before scanning. Representative wells were selected for display.

Immunofluorescence

For experiments analyzing BRCA1 foci, 10⁶ cells were passed through a 70 µm mesh cell strainer (Thermo Fisher, 22363548) and seeded in a single well of a 6-well plate in the presence of doxycycline (2 µg/ml). After 24 h, IAA was added to a final concentration of 1 mM. Cells were irradiated (5 Gy) 2 h after IAA addition, trypsinized 2 h after irradiation, and 10⁵ cells were plated on fibronectin-coated glass coverslips (13 mm) using a cytopsin. Coverslips were immediately moved to ice cold cytoskeletal buffer (10mM PIPES pH 6.8, 300mM sucrose, 50mM NaCl, 3mM EDTA, 0.5% Triton X-100, Protease Inhibitor Cocktail [cOmplete™ EDTA-free; Roche, 27368400]) for 5 minutes before fixation in 2% PFA. *BARD1*^{AID/AID} *53bp1*^{-/-} cells stably transduced with 53BP1-BARD1 fusion protein were prepared identically as described for BRCA1 foci, but were immediately fixed in 2% PFA after cytopsin. After fixation, these cells were permeabilized in PBS containing 0.2% Triton X-100. For analysis of BRCA1 foci in *RNF168*^{-/-}, *PRC1*^{-/-}, and *BARD1*^{R99E} cells (Extended Data Fig. 4c-g), 2x10⁵ cells were passed through a 70 µm mesh cell strainer and seeded on 3 fibronectin-coated glass coverslips (13 mm) in a single well of a 6-well plate in the presence of doxycycline (2 µg/ml). After 24 h, IAA was added to a final concentration of 1 mM. 2 h after IAA, cultures were treated with 40 µM EdU for 10 min. EdU was washed out with fresh medium and the cells were immediately irradiated (5 Gy), then fixed in 2% PFA 2 h after irradiation.

We found RAD51 foci staining to be disrupted by cytopsin plating. For RAD51 foci quantification, 2x10⁵ cells were passed through a 70 µm mesh cell strainer and seeded on 3 fibronectin-coated glass coverslips (13 mm) in a single well of a 6-well plate in the presence

of doxycycline (2 µg/ml). After 24 h, IAA was added to a final concentration of 1 mM. Cells were irradiated (5 Gy) 2 h after IAA addition and fixed in 2% PFA 2 h after irradiation.

Staining of all fixed cells began with 15 min blocking (3% BSA, 0.1% Triton X-100 in PBS), followed by 1 h incubation with primary antibody in a humidity chamber. For experiments in which cells were treated with EdU, the Click-iT™ EdU Cell Proliferation Kit, Alexa Fluor™ 647 (Thermo Fisher, C10340) was used to label EdU positive cells according to the manufacturer's protocol between blocking and primary antibody incubation. The following primary antibodies were used at the indicated concentrations: mouse anti-HA (1:200, HA.11 901501 Biolegend), mouse anti-BRCA1 D-9 (1:40, sc-6954 Santa Cruz), rabbit anti-H4K20me0 (1:250, ab227804 Abcam), rabbit anti-RAD51 (1:1000, 70-001 BioAcademia), mouse anti-γH2AX (1:500, 05-636 Millipore), rabbit anti-53BP1 (1:250, NB100-304), and rabbit anti-γH2AX (1:500, 2212-1 Epitomics). Following primary, coverslips were washed 3 times with PBS containing 0.1% Triton X-100 before incubation with secondary antibody for 1 h in a humidity chamber. Secondary antibodies used in this study were: goat anti-mouse Alexa Fluor 488 (1:500, A-11001 Invitrogen) and goat anti-rabbit Alexa Fluor 568 (1:500, A-11011 Invitrogen). Coverslips were then washed 3 more times with PBS containing 0.1% Triton X-100, once with PBS, and mounted on glass microscope slides using a drop of ProLong® Gold antifade reagent with DAPI (Life Technologies, P36935).

Live imaging of *BARD1^{AID/AID}* cells expressing mC2-ARD-BRCT fusion transgenes was performed using Leica SP8-X SMD confocal microscope. For each cell line, 10⁵ cells were seeded in duplicate on 35 mm glass-bottomed dishes in the presence of doxycycline (2 µg/ml). IAA (1 mM) was added after 24 h and cells were irradiated (10 Gy) 2 h later. Imaging began 1 h after irradiation and continued for 30 min.

Immunofluorescence images for BRCA1 quantification were acquired on a Leica DMI8 widefield microscope (Fig. 2d-g and Extended Data Fig. 2d-g) or Leica SP8-X SMD confocal microscope (Extended Data Fig. 4c-g). 53BP1-BARD1 fusion protein experiments were visualized on a Leica SP8-X SMD confocal microscope. CellProfiler (Broad Institute) was used for foci quantification. Images were visualized and saved in Fiji and assembled into figures in Adobe Illustrator.

Protein extraction and western blotting

Cells were washed once with PBS and lysed by resuspension in ice cold benzonase cell lysis buffer (40 mM NaCl, 25 mM Tris pH 8.0, 0.05% SDS, 2 mM MgCl₂, 10 U/ml benzonase, and cOmplete™ EDTA-free protease inhibitor cocktail [Roche, 27368400]). Extracts were then incubated on ice for 10 min before protein concentration was calculated

by Bradford assay (Bio-Rad, 500-0006). Extracts were then mixed with Laemmli buffer and boiled at 95°C for 5 minutes before loading on SDS-PAGE gels.

Protein samples were fractionated on NuPAGE™ 4-12% 1.0 mm Bis-Tris polyacrylamide gels (Life Technologies, NP0322) before transferring to 0.45 µm nitrocellulose membranes (GE Healthcare, 10600003). After transfer, membranes were blocked with 5% milk in PBST for at least 30 min and then incubated overnight with primary antibody in PBST supplemented with 0.03% NaN₃ and 3% BSA. Primary antibodies used for western blot in this study include: rabbit anti-53BP1 (1:2500, Novus Biological, NB100-304), mouse anti-BRCA1 D-9 (1:400, sc-6954 Santa Cruz), rabbit anti-BARD1 (1:500, ab64164 Abcam), mouse anti-β-actin (1:2000, A1978 Sigma-Aldrich), rabbit anti-RING1B D22F2 (1:1000, 5694 Cell Signaling), rabbit anti-H2A-K119-Ub D27C4 (1:2000, 8240S Cell Signaling), rabbit anti-CHK2-Phospho-Thr-68 C13C1 (1:1000, 2197 Cell Signaling), rabbit anti-H2AX (1:1000, ab124781 Abcam; also recognises H2A), and mouse anti-HA (1:2000, HA.11 901501 Biolegend). Following primary, membranes were incubated with either HRP-conjugated goat anti-mouse (1:20,000, Thermo Fisher, 62-6520) or HRP-conjugated goat anti-rabbit (1:20,000, Thermo Fisher, 65-6120) secondary antibodies. Membranes were developed with Clarity™ Western ECL Substrate (Bio-Rad, 170-5061) and imaged using a Gel Doc™ XR System (Bio-Rad).

For nucleosome pull-down assays, proteins were separated using 4-20% tris glycine gradient gels (BioRad) prior to transfer onto PVDF membranes. All blocking and antibody incubations were performed in Tris-buffered saline containing either 5% (w/v) BSA or 5% (w/v) skimmed milk powder. For Western blotting the following commercial primary antibodies were used: rabbit anti-H2A (Abcam, ab18255), rabbit anti-H3 (Abcam, ab1791), mouse anti-GST (Santa Cruz, sc-138). HRP-conjugated goat anti-rabbit IgG (Vector Laboratories, PI-1000) and HRP-conjugated horse anti-mouse IgG (Vector Laboratories, PI-2000) secondary antibodies were used with enhanced chemiluminescence solution (ECL supersignal, Thermo Scientific) was used for protein detection.

Protein purification

GST₂, GST-BARD1^{ARD-BRCT}, and 6xHis-MBP-BARD1^{ARD-BRCT} (corresponding to residues 425-777) variants were expressed using 200µM IPTG in BL-21 DE3 RIL *E. coli* overnight cultures grown at 16°C in 2YT broth. Cell pellets were resuspended in lysis buffer (25mM Tris pH 8, 300mM NaCl, 0.1% Triton (v/v), 10% glycerol (v/v), 5 mM β-mercaptoethanol, 1× Protease Inhibitor mix [284 ng/ml leupeptin, 1.37 µg/ml pepstatin A, 170 µg/ml phenylmethylsulfonyl fluoride and 330 µg/ml benzamidine], 1mM AEBSF and 5 µg/ml DNaseI). Cells were lysed by sonication and lysozyme treatment and spun at 39000g for 30 minutes. For GST tagged proteins, clarified lysate was applied to a Glutathione Sepharose 4B

column (GE Healthcare). After extensive washing, bound protein was eluted using 30mM reduced glutathione and concentrated using a 30K MWCO centrifugation device (Amicon). 6xHis-MBP-BARD1^{ARD-BRCT} lysates were treated the same, with the addition of 15mM Imidazole to the buffer after lysis. 6xHis-MBP-BARD1^{ARD-BRCT} was applied to a chelating HP column (GE Healthcare) preloaded with Nickel ions. After extensive washing, protein was eluted using a gradient of Imidazole (15 Column volumes final Imidazole concentration 300mM). Proteins were further purified by size exclusion chromatography using a Superdex 200 Increase 10/300 in SEC buffer (20mM Tris pH 7.5, 150mM NaCl, 1mM DTT, 5 % glycerol) and the main mono-disperse protein containing peak was collected, concentrated, flash frozen in liquid nitrogen and stored at -80°C. GST-53BP1^{TTD-UDR} (residues 1484-1631) was expressed and purified as described⁵.

Protein concentrations were determined via absorbance at 280 nm using a Nanodrop 8000 (Thermo Scientific), followed by SDS-PAGE and InstantBlue (Expedeon) staining with comparison to known amounts of control proteins (Extended Data Fig. 3c and 3f).

Human histone proteins including site specific cysteine mutations were expressed in BL-21 DE3 RIL cells and purified from inclusion bodies, essentially as described^{5,37}. 6xHis-TEV-ub G76C was expressed in *E. coli* BL-21 DE3 CodonPlus cells, lysed in 1xRecom-500 buffer (25 mM Na-Phosphate buffer pH 7.4, 300 mM NaCl, 0.1% [v/v] Triton, 10% [v/v] glycerol, 4 mM β -mercapthoethanol, 1x Protease Inhibitor mix, 5 μ g/ml DNaseI) and treated with lysozyme and sonication. Clarified cell lysate was loaded onto a HiTrap chelating column (GE Healthcare) pre-loaded with Ni²⁺ ions. After extensive washing, 6xHis-TEV-ub was eluted using a gradient of imidazole and peak-protein containing fractions were concentrated using a 3K MWCO centrifugation device (Amicon). 6xHis-TEV-ub was further purified on a S75 10/300 column in SEC buffer. Protein-containing fractions were dialyzed into water supplemented with 1 mM acetic acid prior to lyophilization.

H4 Methyl lysine analog preparation

H4K20C was expressed and purified as described for other histones. Cysteine-engineered histone H4K20C protein was alkylated essentially as described³⁸. Briefly, pure histone H4 was reduced with DTT prior to addition of a 50-fold molar excess of (2-chloroethyl) dimethylammonium chloride (Sigma-Aldrich). The reaction was allowed to proceed for four hours at room temperature before quenching with 5 mM β -mercaptoethanol. The H4 protein was separated and desalted using a PD-10 desalting column (GE Healthcare), pre-equilibrated in water supplemented with 1mM acetic acid and lyophilized. After incorporation of alkylation agents was assessed by 1D intact weight ESI mass spectrometry, roughly 85% was found to be modified. Lyophilized H4 was subject to a second round of alkylation as described above with the final reaction proceeding to near completion (~95%).

H2A chemical ubiquitylation

Mutant human histone H2A engineered with a single cross-linkable cysteine (H2A K15C or K119C) was chemically ubiquitylated essentially as described^{5,39}. Briefly, an alkylation reaction was assembled with an H2A cysteine mutant (700uM), 6xHis-TEV-ubiquitin G76C (700uM) and 1,3-dibromoacetone (4.2mM, Santa Cruz) in 250 mM Tris-Cl pH 8.6, 8 M urea and 5 mM TCEP and allowed to react for 16 hours on ice. The reaction was quenched by the addition of 10 mM β -mercaptoethanol and pH adjusted to 7.5. Chemically ubiquitylated H2A (H2A Kc15ub or H2A Kc119ub) was purified using a HiTrap SP HP column (GE Healthcare) and 6xHis-TEV-H2AKc15ub containing fractions were pooled and enriched over a HiTrap chelating column (GE Healthcare) pre-loaded with Ni^{2+} ions. The 6xHis tag was removed by TEV cleavage and subsequent Ni^{2+} column subtraction. The resulting flow-through was dialysed against a 2mM β -mercaptoethanol/dH₂O solution and lyophilized. H2AKc15ub was refolded and wrapped into nucleosomes as described below.

Nucleosome reconstitution

Nucleosomes were reconstituted essentially as described^{5,37}. Biotinylated 175bp Widom-601 DNA fragments for wrapping nucleosomes were generated by PCR based amplification, essentially as described⁴⁰. For PCR amplification, 384 100ul reactions PCR reactions using Pfu polymerase and HPLC pure oligos (IDT) were pooled, filtered and purified using a ResourceQ column and salt gradient.

For octamer formation, 4 core histones were mixed at equimolar ratios in unfolding buffer (7M Guanidine HCl, 20mM Tris pH 7.5, 5mM DTT) prior to dialysis to promote refolding into 2M NaCl, 15mM Tris pH 7.5, 1mM EDTA, 5mM β -mercaptoethanol. Octamers were selected by gel filtration chromatography and assembled into nucleosomes via salt gradient dialysis. Soluble nucleosomes were partially precipitated with 9% polyethylene glycol (PEG) 6000 and resuspended in 10mM HEPES pH7.5, 100mM NaCl, 1mM EDTA, 1mM DTT. Nucleosome formation and quality was checked by native gel electrophoresis and used within one month of wrapping (Extended Data Fig. 3e).

Nucleosome Pull-down assays

Pull-down assays were performed essentially as described⁵. Briefly, 2.5 μg of GST-tagged 53BP1^{TTD-UDR} or 8.5 μg of GST-BARD1^{ARD-BRCT}/GST₂ was immobilized on BSA-blocked Glutathione sepharose beads. Beads were separated and incubated with 2.2 μg of nucleosome variant in pull-down buffer (50 mM Tris-HCL pH 7.5, 150mM NaCl, 0.02% NP40, 0.1 mg/ml BSA, 10 % glycerol, 1mM EDTA, 2mM β -mercaptoethanol) for 2 hours with rotation

at 4°C. Pull-downs were washed three times in pull-down buffer and resuspended directly in 2× SDS loading buffer. All pull-down assays were repeated at least two times, with a single representative immunoblot displayed.

Modified nucleosomes binding assays (EMSA)

20nM of either H2AKc15ubmodified nucleosomes, H4Kc20me2 H2AKc15ub modified nucleosomes, or 175bp Widom-601 DNA (the same DNA used to wrap nucleosomes) was incubated with serial dilutions of recombinant 6xHis-MBP-BARD1^{ARD-BRCT} to a final volume of 20ul in EMSA buffer (15mM Tris pH 7.5, 75mM NaCl, 0.05mg/ml BSA, 0.5mM EDTA, 10% glycerol, 0.05% triton X-100, 1mM DTT, 8% sucrose, 0.01% bromophenol blue). Samples were incubated at 4°C for 45 minutes to ensure end point of binding was reached. Products were separated on a native 5% polyacrylamide gel with 0.5x TBE as the running buffer for 2 hours at 4°C. Gels were stained using Diamond DNA stain (Promega). Binding was estimated based on the disappearance of the band corresponding to nucleosome or free DNA and quantified in Image Lab (BioRAD, version 6.1). Binding curves and apparent binding affinity were determined in GraphPad Prism (version 9), using non-linear regression analysis. EMSA assays were repeated at least in triplicate.

Statistics

Prism 9 (Graphpad Software Inc.) was used for graphing and statistical analysis. Relevant statistical methods for individual experiments are detailed within figure legends.

- 37 Dyer, P. N. *et al.* in *Methods in Enzymology* Vol. 375 23-44 (Academic Press, 2003).
- 38 Simon, M. D. *et al.* The Site-Specific Installation of Methyl-Lysine Analogs into Recombinant Histones. *Cell* **128**, 1003-1012, doi:10.1016/j.cell.2006.12.041 (2007).
- 39 Long, L., Furgason, M. & Yao, T. Generation of nonhydrolyzable ubiquitin-histone mimics. *Methods* **70**, 134-138, doi:10.1016/j.ymeth.2014.07.006 (2014).
- 40 Wilson, M. D. *et al.* Retroviral integration into nucleosomes through DNA looping and sliding along the histone octamer. *Nature Communications* **10**, 4189, doi:10.1038/s41467-019-12007-w (2019).

Extended Data Fig. 1. BARD1 BRCT-mutated transgenes are stably expressed in *BARD1^{AID/AID}* HCT-116 cells (related to Figure 1). (A) Immunoblots of whole cell lysates harvested at the indicated timepoints after IAA addition. Expression of the auxin-degron-targeting SCF-complex E3 ligase OsTIR1 was induced using doxycycline (2 µg/ml), 24 h prior to the depletion of endogenous BARD-AID protein with IAA (1 mM). Representative of two biological repeats. (B) Immunoblot from whole cell lysates of BARD1 BRCT mutants screened for olaparib sensitivity. (C) Immunoblot of whole cell lysates from *BARD1^{AID/AID}* expressing the indicated transgenes. Cells were seeded in the presence of doxycycline (2 µg/ml) and IAA (1 mM) was added after 24 h. Lysates were harvested at the indicated timepoints after IAA addition. Representative of two biological repeats.

Extended Data Fig. 2. Ankyrin and BRCT repeat domains in BARD1 cooperate in recruiting BRCA1 to post-replicative chromatin during HR. (Related to Figure 2). (A-C) Survival of indicated *BARD1^{AID/AID}* cell lines grown for 7 days without IAA in the presence of indicated doses of olaparib or cisplatin. Cell lines were seeded in doxycycline (2 µg/ml) for 24 h before olaparib or cisplatin addition. Resazurin cell viability assay, *n*=3 biological experiments, mean ±SD. (D) High-content immunofluorescent microscopy of BRCA1 IRIF in H4K20me0-positive *BARD1^{AID/AID}* cells expressing the indicated transgenes. Cultures were grown in the presence of doxycycline (2 µg/ml) for 24 h before IAA (1 mM) addition, irradiated 2 h later, and fixed following irradiation. Scale bar, 5 µm. Representative of *n*=2 biological experiments. (E) *Top*: quantification of BRCA1 IRIF from (D). Boxes indicate the 25th-75th percentiles with the median denoted and whiskers indicate the 10th-90th percentiles. BRCA1 foci measurements are made for nuclei in the bottom quartile of H4K20me0 integrated staining intensity (≥172 nuclei per condition). Foci quantification and H4K20me0 integrated intensity measurements were performed with CellProfiler. *Bottom*: Mean number of BRCA1 foci per cell from two independent experiments ±SD. (F and G) Same as in (D and E) in *rap80^{-/-}* cells. ≥179 nuclei per condition. (H and I) Survival of indicated *BARD1^{AID/AID}* cell lines grown for 7 days without IAA in the presence of olaparib. Cell lines were seeded in doxycycline (2 µg/ml) for 24 h before olaparib addition. Resazurin cell viability assay, *n*=3 biological experiments, mean ±SD.

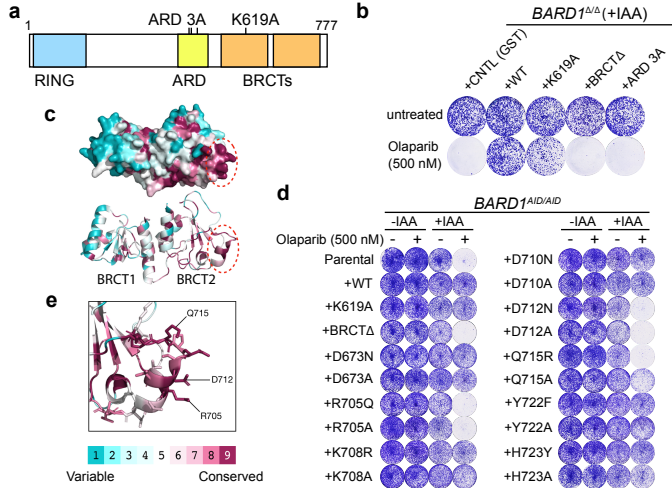
Extended Data Fig. 3. Purification of BARD1 and 53BP1 fragments and assembly of modified nucleosomes (Related to Figure 3). (A) Western blot of HA-tagged 53BP1-BARD1 fusion proteins used in Fig. 5A stably expressed in *BARD1^{AID/AID} 53bp1^{-/-}* cells. (B) *Top*: Model depicting the 53BP1-BARD1 fusion protein. The fusion is a chimera composed of the 53BP1 minimal focus forming region (a.a. 1220-1711) and BARD1 BRCTs (a.a. 555-777). Expressed

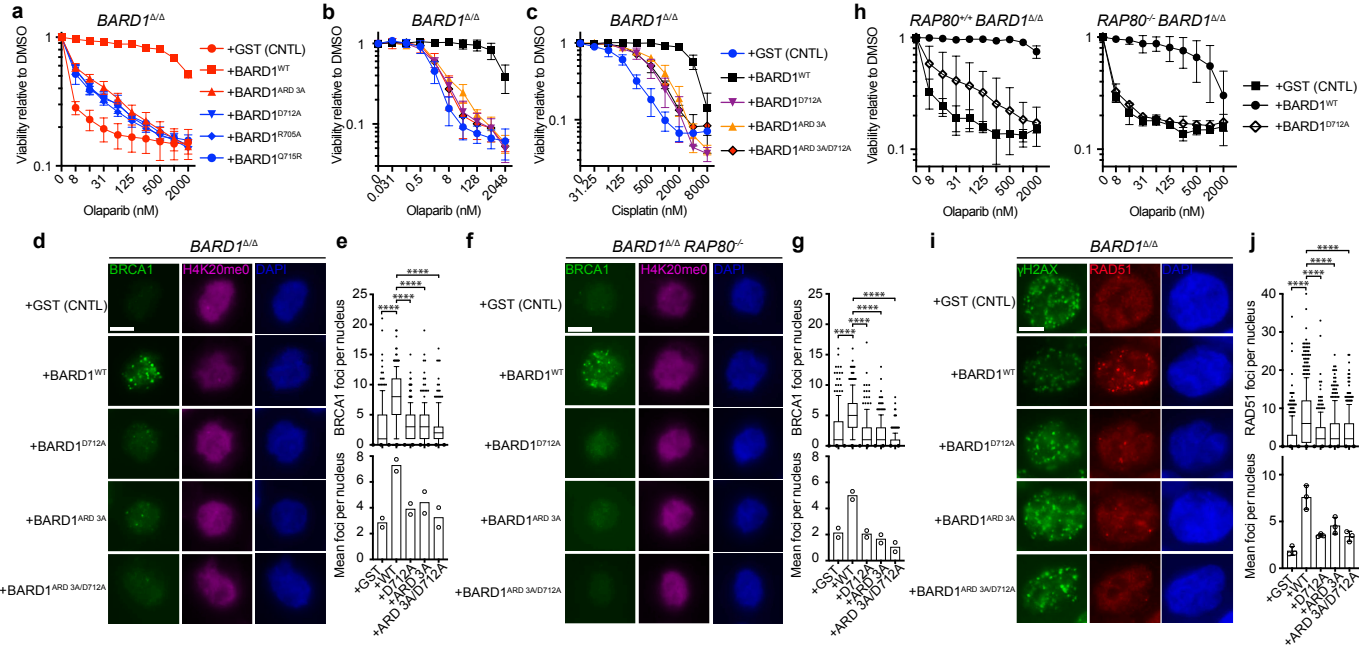
form includes an N-terminal 2xHA-FLAG epitope tag. *Bottom*: Confocal immunofluorescent microscopy of 53BP1-BARD1 chimeric fusion proteins in irradiated *BARD1^{AID/AID} 53BP1^{-/-}* cells. Cultures were grown in the presence of doxycycline (2 µg/ml) for 24 h before IAA (1 mM) addition and irradiated (5 Gy) 2 h later. Cells were fixed 2 h following irradiation. Scale bar, 10 µm. Representative of *n*=2 biological experiments. **(C)** SDS-PAGE gel, stained with InstantBlue protein stain of proteins used in Fig. 3A. **(D)** SDS-PAGE gel, stained with InstantBlue protein stain of nucleosomes used in this study. **(E)** Native gel electrophoresis of Widom 601 DNA in isolation and wrapped with nucleosomes used in this study. **(F)** Representative gel images from EMSA experiments quantified in Fig. 3B. H2AKc15ub or H2AKc15ubH4Kc20me2 modified nucleosomes (or control DNA) were incubated with increasing concentrations of 6xHis-MBP-BARD1^{ARD-BRCT} or GST-53BP1^{TTD-UDR}. Complexes were resolved by native PAGE and visualized using Diamond DNA stain. **(G)** SDS-PAGE gel, stained with InstantBlue protein stain of BARD1 variants used in Fig. 3C. Neighbouring lanes were loaded with two different concentrations.

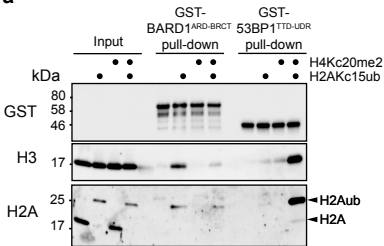
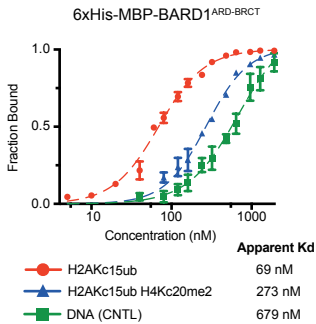
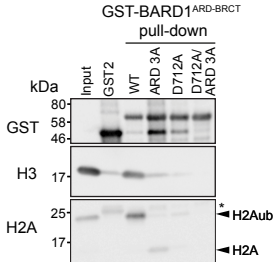
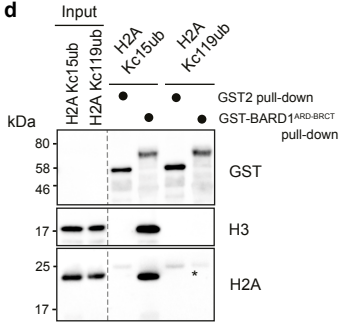
Extended Data Fig. 4. BRCA1 recruitment to IRIF is RNF168-dependent, but independent of PRC1 and BRCA1-BARD1 ubiquitin ligase activity (related to Figure 4).

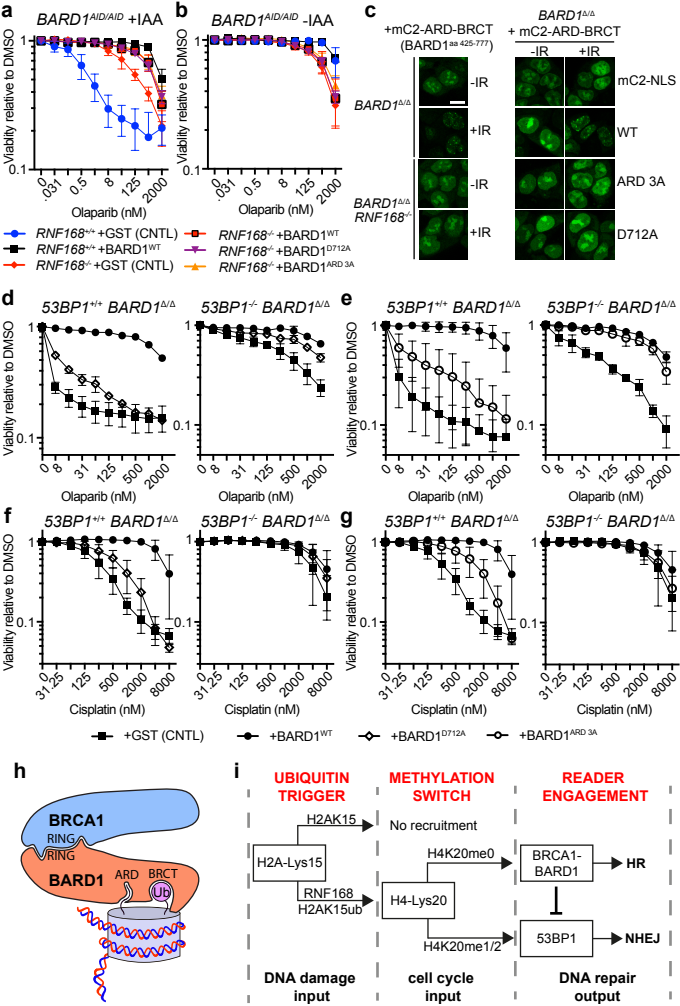
(A) Model indicating the three major known sites of ubiquitin attachment on histone H2A and the genetic manipulations used to block each individually in our experiments. *PRC1^{-/-}* indicates *RING1A^{-/-} RING1B^{-/-}* double knockout. **(B)** Immunoblot of whole cell lysates from *BARD1^{AID/AID}* parental cells and *RNF168^{-/-}* derivatives. Cells were seeded in the presence of doxycycline (2 µg/ml) and IAA (1 mM) was added after 24 h. Lysates were harvested 8 h after IAA addition. Representative of two biological repeats. **(C)** Immunofluorescent microscopy of *BARD1^{AID/AID}* parental cells and *RNF168^{-/-}* derivatives. Cultures were seeded 24 h before irradiation (5 Gy), and fixed 2 h later. Representative of *n*=3 biological experiments. Scale bar, 10 µm. **(D)** Quantification of BRCA1 and 53BP1 IRIF from (C). Boxes indicate the 25th-75th percentiles with the median denoted and whiskers indicate the 10th-90th percentiles. BRCA1 foci measurements are made for EdU positive nuclei. Foci quantification was performed using CellProfiler. Significance was determined by two-sided Kruskal-Wallis H test with Dunn's correction for multiple comparisons (*****p* ≤ 0.0001). Representative of *n*=3 biological replicates. **(E)** Immunoblot of whole cell lysates from *BARD1^{AID/AID}* parental cells *RING1A^{-/-}*, *RING1B^{-/-}*, and *RING1A^{-/-} RING1B^{-/-}* (denoted as *PRC1^{-/-}*) derivatives. Cultures were seeded 24 h before irradiation (10 Gy), and harvested 2 h later. **(F and G)** The indicated cell lines were treated as in (D). Representative of *n*=3 biological replicates.

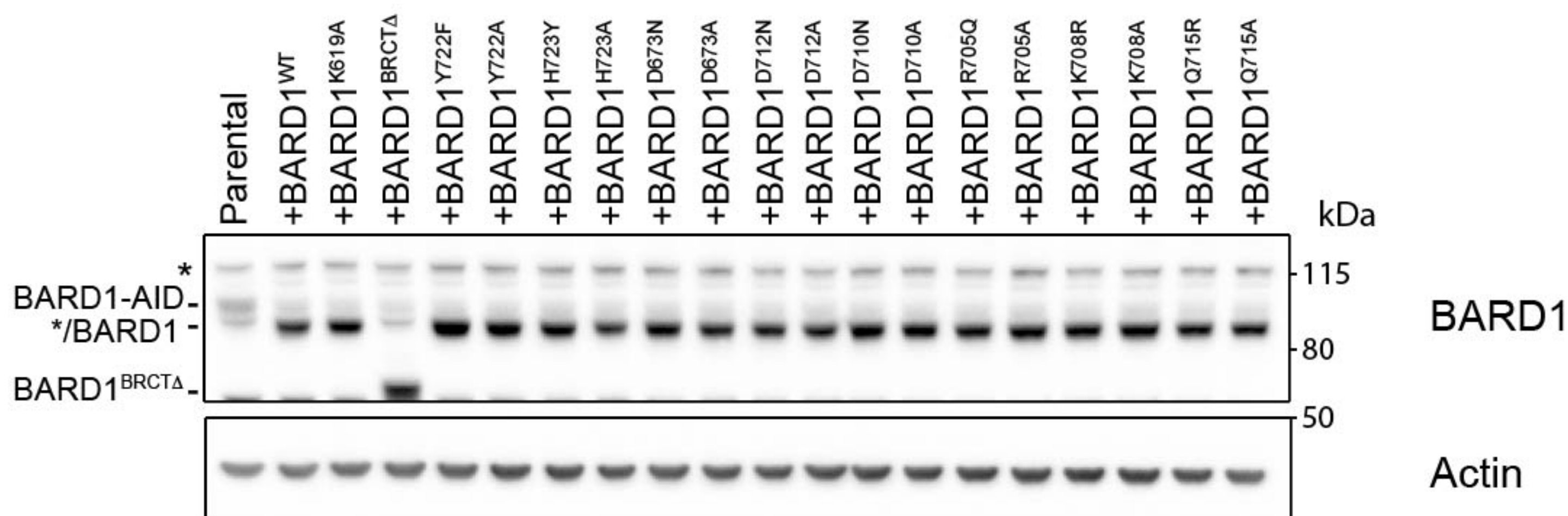
Extended Data Fig. 5. The $\beta 2'$ - $\beta 3'$ loop and ARD counteract toxic 53BP1-dependent NHEJ (related to Figure 4). **(A)** Immunofluorescent microscopy of RAD51 IRIF in *BARD1^{AID/AID}* cells expressing the indicated transgenes. Cultures were grown in the presence of doxycycline (2 μ g/ml) for 24 h before IAA (1 mM) addition, irradiated 2 h later (5 Gy), and fixed with PFA 2 h following irradiation. Data was collected from the same experiment as Fig. 2I-J. Scale bar, 5 μ m. Representative of $n=3$ biological experiments. **(B) Top:** Quantification of Rad51 foci per cell from (A). ≥ 255 nuclei per condition. Boxes indicate the 25th-75th percentiles with the median denoted and whiskers indicate the 10th-90th percentiles. Significance was determined by two-sided Kruskal-Wallis H test with Dunn's correction for multiple comparisons (**** $p \leq 0.0001$, *** $p = 0.0003$). Data is from same experiment presented in Figure 2i-j. *BARD1^{AID/AID}* cells expressing GST and *BARD1^{WT}* are displayed in both for comparison. Representative of $n=3$ biological experiments. **Bottom:** Mean number of RAD51 IRIF from three independent biological experiments \pm SD. **(C and D)** Immunoblot of whole cell lysates from *BARD1^{AID/AID}* (top) or *BARD1^{AID/AID} 53BP1^{-/-}* (bottom) cells expressing the indicated transgenes. Cells were seeded in the presence of doxycycline (2 μ g/ml) and IAA (1 mM) was added after 24 h. Lysates were harvested at the indicated timepoints after IAA addition. Representative of two biological repeats. **(E-H)** Survival of indicated *BARD1^{AID/AID}* cell lines grown without IAA for 7 days in the presence of indicated doses of olaparib or cisplatin. Cultures were seeded in doxycycline (2 μ g/ml) and olaparib or cisplatin was added 24 h later. Survival was measured after 7 days by resazurin cell viability assay ($n=3$ biological experiments) mean \pm SD.





a**b****c****d**



a*BARD1*^{AID/AID}**b***BARD1*^{AID/AID}**c***BARD1*^{AID/AID}